This is the peer-reviewed, final accepted version for American Mineralogist, published by the Mineralogical Society of America.
The published version is subject to change. Cite as Authors (Year) Title. American Mineralogist, in press.
DOI: https://doi.org/10.2138/am-2021-7868. http://www.minsocam.org/

Revision 1 of manuscript #7868

Fluorine partitioning between quadrilateral clinopyroxenes and melt

Don R. Baker[1], Sara Callegaro[2], Angelo De Min[3], Martin J. Whitehouse[4], Andrea Marzoli[5]

[1]McGill University, Department of Earth and Planetary Sciences, Montréal, Quebec, Canada.

[2]Centre for Earth Evolution and Dynamics (CEED), University of Oslo, PO Box 1028, Blindern N-0316 Oslo, Norway.

[3]Department of Mathematics and Geoscience, University of Trieste, via Weiss 2, 34128 Trieste, Italy

[4]Swedish Museum of Natural History, Stockholm, Sweden

[5]University of Padova, Department of Land, Environment, Agriculture and Forestry, Padova, Italy

DEDICATED TO THE MEMORY OF JIM WEBSTER FOR HIS WISDOM, WIT, AND KINDNESS

Corresponding author: don.baker@mcgill.ca

Keywords: mineral/melt partitioning, fluorine, chlorine, silicate melt, clinopyroxene partition coefficient

ABSTRACT

Concentrations of fluorine and chlorine were measured in glasses (quenched melts) and coexisting clinopyroxene, orthopyroxene, olivine, and plagioclase in run products of experiments previously used to measure sulfur partitioning between these phases. The partitioning of F between clinopyroxene and silicate melt was determined in 13 experiments at a variety of pressures, temperatures, and melt compositions ranging from basaltic to dacitic (49 to 66 wt.% SiO_2) at 0.8 to 1.2 GPa and 1000 to 1240 °C, at hydrous and anhydrous conditions. Additionally, we determined the crystal-melt partitioning of F

This is the peer-reviewed, final accepted version for American Mineralogist, published by the Mineralogical Society of America.
The published version is subject to change. Cite as Authors (Year) Title. American Mineralogist, in press.
DOI: https://doi.org/10.2138/am-2021-7868. http://www.minsocam.org/

for 4 experiments with plagioclase, 2 with orthopyroxene, and 1 with olivine. Although Cl was also measured in the experiments, the concentrations in the crystals are close to background concentration levels. The partition coefficients of fluorine between clinopyroxene and melt varied from ~0.09 to 0.29 and were linearly dependent upon the concentration of aluminum in the octahedral M1 site of clinopyroxene. Similar relationships are seen when our results are combined with previous measurements of the fluorine partition coefficient between clinopyroxene and melt, but each study shows its unique correlation between the F partition coefficient and Al^{M1}. These dissimilarities in correlations with Al^{M1} are attributed to differing analytical protocols used in the various studies. However, the combined dataset demonstrates a linear correlation with Al^{M1}, the inverse of the NBO/T ratio of the melt (T/NBO), pressure and temperature, which can be described as:

$$\ln(D_F^{cpx/L}) = (0.2298 \pm 0.04847)(T/NBO) - (1.029 \pm 0.8045)(Al^{M1}) - (3889 \pm 1803)(1/T) - (0.5472 \pm 0.1084)(P) + 0.5871 \pm 1.304 \quad ,$$

where each uncertainty is 1 standard error in the fit (as calculated by the R-project software), T is in K and P is in GPa. Although this relationship reproduces 81% of the partitioning data to within 25% (relative), the different linear trends of the partition coefficient, $D_F^{cpx/L}$, versus Al^{M1} from different laboratories suggest the need for additional investigations and development of clinopyroxene standards with certified fluorine compositions. Nevertheless, we conclude that the self-consistency of each study indicates that F partition coefficients determined using one protocol can be applied to minerals or glasses analyzed using the same protocol and ion microprobe to better understand the storage and transport of fluorine in magmatic systems.

This is the peer-reviewed, final accepted version for American Mineralogist, published by the Mineralogical Society of America.
The published version is subject to change. Cite as Authors (Year) Title. American Mineralogist, in press.
DOI: https://doi.org/10.2138/am-2021-7868. http://www.minsocam.org/

INTRODUCTION

The igneous quintet of H_2O, CO_2, F, S, and Cl dominates the volatile budget of terrestrial magmatic systems (e.g., Johnson et al. 1994; Symonds et al. 1994), and degassing from volcanoes can have a profound influence on planetary habitability (e.g., Self et al. 2014). Understanding the storage and transport of these volatiles is the goal of geoscientists seeking to predict the magnitude and occurrence of volcanic eruptions (e.g., Edmonds 2008; Robock 2013; Webster et al. 2018), as well as trying to infer the environmental impacts of past and future igneous events on the history of Earth and life upon its surface (e.g., Wignall 2001; Black et al. 2012; Bond and Wignall 2014; Capriolo et al. 2020). Fluorine is of particular interest because of its presence in igneous rocks throughout the inner solar system (Harlov and Aranovich 2018), and because of its well-known toxic effects (e.g., D'Alessando 2006; Hansell et al. 2006).

Pre-eruptive volatile concentrations are often estimated from analysis of melt inclusions trapped in crystals (e.g., Devine et al. 1984; Johnson et al. 1994; Cannatelli et al. 2016); however, such inclusions reflect rapid growth of the host crystal, possibly under disequilibrium conditions (e.g., Baker 2008), and are rare. When melt inclusions are absent, other approaches must be used. With the advent of tools allowing in situ analysis of small volumes of crystals down to concentrations at the ppm level (e.g., the ion microprobe), the use of the partition coefficients, $D^{crystal/melt}$, of volatiles between nominally volatile-free crystals and melts has started to become a routine technique for the estimation of volatile concentrations in magmatic systems. Partition coefficients for each of the volatiles in the igneous quintet have been determined previously, but only for a small suite of experimental run products (discussed below) and natural samples.

The study reported in this contribution was undertaken to measure fluorine and chlorine partition coefficients between clinopyroxene and melt in experimental run products previously used for the measurement of sulfur partitioning (Callegaro et al. 2020). The goal was to combine the newly acquired partition coefficients with those already present in the literature to resolve differences between previously measured partition coefficients, which can reach a factor of 5 (cf., Hauri et al. 2006 and Guggino 2012) and to create a universal model to predict the partition coefficient of fluorine between quadrilateral clinopyroxenes and melt. As will be shown below, that goal was not entirely reached because of apparent inter-laboratory differences. However, we found evidence for intra-laboratory consistency and show that models exist that can relate the clinopyroxene and melt compositions to the measured fluorine partition coefficient. These partition coefficients can then be used to evaluate pre-eruptive concentrations of fluorine in magmatic systems from clinopyroxene analyses made using the same protocol, and ideally the same instrument, as used to measure the partition coefficients.

EXPERIMENTAL AND ANALYTICAL TECHNIQUES

Halogen concentrations in crystals and quenched melts were measured in experimental run products previously used to determine sulfur partitioning between crystals and melts (Callegaro et al. 2020). Details of the experimental techniques, attainment of equilibrium, and complete major and minor element analyses of the experimental run products are provided in Callegaro et al. (2020), so only a brief summary is provided here.

Crystallization experiments were performed using bulk compositions ranging from basaltic to dacitic at pressures from 0.8 to 1.2 GPa in a piston-cylinder apparatus using a NaCl-pyrex assembly and following the techniques described in Baker (2004). The bulk compositions studied were a Mid-Ocean Ridge Basalt (MORB), a primitive basalt collected from a lava flow of the Central Atlantic Magmatic Province sampled in Morocco, an andesitic glass produced from an Aleutian island sample

that was doped with diopside glass (AT-29D), and a synthetic dacitic glass (AT-150). The major element compositions of the starting materials are provided in the Online Material. Experimental temperatures were between 1000 and 1240 °C, where high-temperature experiments were anhydrous and low-temperature ones hydrous (Callegaro et al. 2020).

Low oxygen fugacity experiments were performed in graphite-lined Pt capsules and high oxygen fugacity experiments in $Au_{75}Pd_{25}$ capsules. Oxygen fugacities in the $Au_{75}Pd_{25}$ capsules were measured using the peak shift of sulfur due to its changing speciation in the melt from S^{2-} to S^{6+} with increasing oxygen fugacity as measured on the electron microprobe (Callegaro et al. 2020). Experiments performed in graphite-lined Pt capsules had no discernible S^{6+} and the oxygen fugacity is estimated at two log units below the fayalite-magnetite-quartz buffer (Callegaro et al. 2020). High oxygen fugacity experiments were ~1 to 2 log units above the fayalite-magnetite quartz buffer.

Experiments were simultaneously raised to super-liquidus pressure-temperature conditions and remained there for 1 to 2 h to completely melt each starting material and homogenize the melt. Subsequently the experiments were cooled to subliquidus conditions at a rate of 1 °C per minute. Once the experiments reached the targeted crystallization temperatures they were maintained at that temperature for a duration of approximately 24 h, during which crystal growth occurred (Table 1). Previous studies (Baker and Eggler 1987; Baker 2008) have demonstrated that this duration is sufficient for the andesite AT-29 and the MORB basalt to reach equilibrium conditions at anhydrous conditions and similar temperatures and pressures, even with residual melt compositions as rich in silica (67 wt% SiO_2) as those in this study.

Fluorine and chlorine concentrations in the experimental crystals and quenched melts mounted in Epofix® epoxy were measured by Secondary Ion Mass Spectrometry (SIMS) using a large geometry CAMECA IMS 1280 instrument at the Nordsim facility, Swedish Museum of Natural History,

Stockholm (Sweden). The analytical protocol was modified slightly from that previously described for halogen concentration measurements in phosphates by removal of the Br and I isotopes (Kusebauch et al. 2015). A Gaussian-focused $^{133}Cs^{+}$ primary beam of ~0.5 nA with an accelerating voltage of -10 kV was used together with low-energy, normal-incidence electron flooding to counteract charge buildup on the target. At the beginning of each analysis the primary beam was rastered over a 20 x 20 μm square area for 120 seconds prior to data acquisition to remove the gold coating and surface contamination, then reduced to a ~10 x 10 μm raster during data acquisition in order to produce a relatively flat-bottomed crater profile and thus ensure consistent secondary ion emission throughout the analysis. Secondary ions were accelerated using a potential of -10 kV, centered in the field aperture and optimized for mass calibration using the ^{18}O signal. Secondary ion species at a mass resolution (M/Δ M) of 2430 were then measured by magnet peak switching on a low-noise, ion-counting electron multiplier. Halogen concentrations were determined from the ratios of $^{19}F/^{18}O$ and $^{35}Cl/^{18}O$ and calibrations that plotted the fluorine or chlorine concentration (in ppm) as a function of the appropriate ratio. Oxygen was chosen because of its similar concentrations in both the samples and the standards. The fluorine working curve utilized the ATHO-G and T1-G glasses with concentrations of 1006 ppm and 233 ppm, respectively (E. Rose-Koga, Univ. Blaise Pascal, Clermont Ferrand, pers. comm. 2016), while the Cl working curve used ATHO-G and T1-G with concentrations of 424 ppm (E. Rose-Koga, pers. comm., 2016) and 113 ppm (Jochum et al. 2006), respectively, together with the higher concentration B6 glass containing 3300 ppm Cl (Tonarini et al. 2003). In all cases the linear working curves were fitted through the origin (see the Online Material for calibration working curves). Aliquots of many standards have been re-analyzed and new values published for the standards we used (Rose-Koga et al. 2020), but because of possible heterogeneity in the standards we retained the concentrations stated above that were used in 2017, when the measurements were made. We note that changing the concentration of F and Cl in the standard glasses has no effect on the partition coefficient or its

141 standard deviation, but does affect the absolute concentrations of F and Cl in the analyzed crystals and
142 glasses. The standard glasses and reference materials were repeatedly analyzed during the
143 measurements of the run products in this study. External precision based on measurements of reference
144 materials was ±2.8% (n = 32) for F and ±1.0% (n = 16) for Cl; these values were propagated together
145 with the within run uncertainty to yield an estimate of overall uncertainty on the concentration
146 measurements (excluding uncertainty in the reference material concentrations). However, in most
147 cases the uncertainty in the reported concentrations is dominated by the sample standard deviation
148 about the mean value.

149 Detection limits were assessed by assuming a typical detector background of between 0.005 and
150 0.01 cps yielding, respectively, F = 0.039-0.078 ppb and Cl = 0.063-0.126 ppb. We note, however, that
151 these are nominal detection limits based entirely on instrument parameters and do not take into account
152 potential contributions from surface contamination and/or residual gases in the sample chamber. Urann
153 et al. (2017) measured a Herasil® glass sample and a synthetic forsterite (nominally F and Cl free,
154 respectively) on the CAMECA IMS 1280 at the Northeast National Ion Microprobe Facility (Woods
155 Hole Oceanographic Institution) to constrain the effective maximum background values to 0.4 ppm F
156 and 0.3 ppm Cl. Similarly, we measured Cl and F on another Herasil® glass sample. Average
157 concentrations were F=2.1 ppm (± 4.2%) ppm and Cl=1.7 ppm (± 4.0%), where uncertainties are
158 expressed as relative standard deviations. We can conservatively estimate 2.1 ppm F as our maximum
159 background value for fluorine, but since Herasil glass is not considered nominally Cl-free, we cannot
160 follow the same rationale for this element. Furthermore, a comparison of our results with those of
161 Urann et al. (2017) on Herasil® shows that Cl and F concentrations are low but variable among
162 different Herasil® glass samples, and therefore care should be taken when considering this glass as a

163 background monitor. In fact, Cl and F concentrations in Herasil® glass have never been formally
164 certified.

165 **RESULTS**

166 The concentrations of halogens (F and Cl) measured in the quenched melt (glass) and nominally
167 volatile-free crystals are provided in Table 1. Fluorine and chlorine concentrations were measured in
168 clinopyroxenes from 13 experiments, in plagioclases from 4, orthopyroxenes from 2, and olivine from
169 1. The experimental clinopyroxenes were similar to natural igneous crystals with compositions that
170 classify them as quadrilateral clinopyroxenes (Morimoto et al. 1988), as defined by the sum of Ca +
171 Mg + Fe^{2+} and twice the Na in the pyroxene formula (Fig. 1a). The clinopyroxenes produced in the
172 low oxygen fugacity experiments varied from low-calcium pigeonite to augite, whereas clinopyroxenes
173 produced at high oxygen fugacity are augite or diopside (Fig. 1b). The clinopyroxenes produced in the
174 present study are similar to those investigated in previous studies on clinopyroxene/melt partitioning
175 (Fig. 1), although those in this study are sometimes higher in iron (Fig. 1b).

176 The other phases produced in the experiments were also similar to those in nature and
177 previously synthesized in experiments. Plagioclase compositions varied between 60 % albite in one
178 experiment to 64 % anorthite in another. The orthopyroxenes were 86 and 88 % enstatite, and the
179 olivine was 85 % forsterite. The melts produced in the experiments varied from basaltic to dacitic in
180 composition, 49 to 66 wt.% SiO_2 (Callegaro et al. 2020). Most experiments were anhydrous, but those
181 with added water contained 1 to almost 8 wt% water in the quenched glasses (Table 1), as measured by
182 Raman spectroscopy (Callegaro et al. 2020). The complete major element compositions of all phases
183 in these experiments are in Callegaro et al. (2020).

184 The concentrations of F in the melts ranged from approximately 200 to 540 ppm and those of Cl
185 from 54 to 500 ppm. The concentrations of fluorine in the crystals were significantly above the values

186 measured in Herasil® (discussed above) and ranged from ~ 16 to 82 ppm, but chlorine was frequently
187 found at concentrations between 1 and 2 ppm (Table 1), near those of Herasil®, and quite possibly at
188 background levels. The partition coefficients for F between clinopyroxene and melt ranged from 0.09
189 to 0.29, for orthopyroxene from 0.06 to 0.08, and one olivine measurement yielded a value of 0.05
190 (Table 1). The partition coefficients for plagioclase showed a narrow range, varying only from 0.03 to
191 0.05.

192 Chlorine shows much more incompatibility in minerals. Cl partition coefficients between
193 clinopyroxene and melt range from 0.003 to 0.040, between orthopyroxene and melt from 0.001 to
194 0.004, and the single measurement between olivine and melt was 0.003 (Table 1). The Cl partition
195 coefficients for plagioclase were between 0.010 and 0.020. Due to the potentially near-background
196 concentrations of chlorine in the crystals, causing the measured Cl partition coefficients to possibly be
197 maxima, and the few measurements of partition coefficients for orthopyroxene, olivine and plagioclase,
198 we concentrate the discussion on the fluorine partitioning between clinopyroxene and melt.

199

200 ## DISCUSSION

201 ### Controls on fluorine partitioning between clinopyroxene and melt

202 The significant range of fluorine partition coefficients (0.09 to 0.29) between quadrilateral
203 clinopyroxenes and melts measured in this study is similar to previous determinations at similar
204 temperatures and pressures by some authors (Dalou et al. 2012, 2014; Guggino 2012). Nevertheless,
205 other studies have found much smaller variations in the partition coefficients (Hauri et al. 2006,
206 O'Leary et al. 2010; Rosenthal et al. 2015). The spread observed in F partitioning has been previously
207 ascribed to compositional variations in the crystals, in particular the aluminum concentration, and in the
208 melts. We investigate the potential relationships between compositions and our measured F partitioning

by considering the site occupancies in the clinopyroxenes (calculated from microprobe analyses following the schema of Morimoto et al. 1988) and the non-bridging oxygen to tetrahedral cation ratio (NBO/T) of the anhydrous melts following Mysen and Richet (2019).

Fluorine partitioning and Al^{IV} in clinopyroxene. O'Leary et al. (2010) demonstrated a dependence of F partitioning between clinopyroxene and melt upon the tetrahedral aluminum in the clinopyroxene, Al^{IV}; subsequently, other authors demonstrated similar correlations (Dalou et al. 2012; Guggino 2012; Rosenthal et al. 2015), although the exact form of the relationships were not identical. A crystal-chemical rationale for this correlation could be a reaction of Al^{3+} and F^{-} substituting for Si^{4+} and O^{2-}, similar to the suggested mechanism for H^{+} incorporation into clinopyroxene (O'Leary et al. 2010; Dalou et al. 2012; Guggino 2012).

Partition coefficients for our low oxygen fugacity experiments form a linear trend when plotted as a function of Al^{IV} (Fig. 2a). However, the high oxygen fugacity experiments (both hydrous and the one successful anhydrous experiment), which contain higher concentrations of Al^{IV}, are much more scattered and led us to consider other possibilities. One possibility is that the effect of Al^{IV} on F partitioning between high oxygen fugacity clinopyroxene and hydrous melt follows a linear relationship with the same slope as the reduced experiments, but with a different intercept (Fig. 2a). Alternatively, possibly all of the variation in the partition coefficient, $D_F^{cpx/L}$, as a function of Al^{IV} in both oxidized and reduced experiments might be described by a logarithmic relationship (Fig. 2a). However, in both cases the measurements display significant scatter about any line describing their behavior and the differences between the mathematical fit and the measurements can reach a factor of 2*x*. Furthermore, we can offer no theoretical justification for either of these fits.

Fluorine partitioning and Al^{M1} in clinopyroxene. The fluorine partition coefficient correlates with the concentration of Al in the M1 (octahedral) site of clinopyroxene, Al^{M1}, for all of the

measurements, from low oxygen fugacity, low-aluminum pigeonites to high oxygen fugacity, high-aluminum augites (Fig. 2b). The correlation, with a slope of 1.0716 ± 0.2498, reproduces the measured partition coefficients to within 25% (relative) and has a coefficient of determination adjusted for the number of constraints (r^2) of 0.6260. A correlation with Al in the M1 site suggests the possibility of a substitution in which Al^{3+} and F^- in the melt plus a vacancy substitute for two divalent cations on the M1 site (e.g., Fe or Mg) and an oxygen. This reaction was proposed by Guggino in his equation 22 (p. 178 of Guggino 2012), which can be written as:

$$Al^{3+,M1} + F^- + \square \leftrightarrow 2\ M^{2+,M1} + O^{2-}\ , \qquad (1)$$

where □ represents a vacancy in the clinopyroxene structure and $M^{2+,M1}$ represents any 2+ cation in the M1 site. This correlation is consistent with species containing Al and F observed in aluminosilicate melts (Schaller et al. 1992; Zeng and Stebbins 2000; Mysen et al. 2004; Dalou et al. 2015; Mysen and Richet, 2019).

Another alternative might be a jadeite-like substitution (cf., Dalou et al. 2012; Guggino 2012) in which the F partition coefficient increases with increasing Na in the M2 and Al in the M1 site. There is a general increase in $D_F^{cpx/L}$ with Na in the M2 site, but the measurements are scattered (Fig. 2c). The slope obtained, 1.6182 ± 0.9356, is higher than that seen in the correlation of $D_F^{cpx/L}$ with Al in the M1 site (Fig. 2b), although the two slopes are indistinguishable within uncertainty. The presence of Na in the Al-fluoride species of aluminosilicate melts (Schaller et al. 1992; Zeng and Stebbins 2000; Mysen et al. 2004; Dalou et al. 2015; Mysen and Richet, 2019) suggests that a jadeite-like substitution also may play a role in controlling the fluorine partition coefficient.

The association of F with Al in the M1, and possibly Na in the M2, sites of clinopyroxene is consistent with Smyth's (1989) survey of rock-forming, end-member minerals in which he found that F did not enter cation-coordinating polyhedra with less than 6 anions. We suggest that Smyth's (1989)

argument that hydroxyl substitution in nominally volatile-free minerals replaces oxygens with the lowest electrostatic potential in the structure can be extended to fluorine. Applying this hypothesis to diopside and hedenbergite suggests that fluorine replaces oxygen on the O1 site. However, in jadeite the oxygen site with the lowest electrostatic potential is the O2 site. This change in the site with the minimum electrostatic energy of oxygen anions may imply a changing mechanism for fluorine incorporation into clinopyroxene with increasing soda and alumina concentrations.

Correlation of fluorine partitioning with other aspects of clinopyroxene chemistry and melt composition. The possibilities of the partition coefficient being influenced by the Mg# (molar $Mg/Mg + Fe^{total}$), the Fe^{3+} in the M1 site, and the NBO/T ratio of the melt were also investigated (Figs. 2d, e, and f). The Mg number was considered because of the well-known Fe-F avoidance in hydrous minerals (see review by Webster et al. 2018), but no evidence of such avoidance can be seen in tour experimental results (Fig. 2d). Similarly, the concentration of Fe^{3+} in the M1 site, calculated by stoichiometry and charge balance to 6 oxygen atoms in the clinopyroxene formula, does not demonstrate a correlation with $D_F^{cpx/L}$ (Fig. 1e). Lastly, the anhydrous NBO/T ratio does not have a discernible effect on the partitioning of fluorine between clinopyroxene and melt in our experiments (Fig. 2f), although Guggino (2012) and Dalou et al. (2014) found correlations between NBO/T and $D_F^{cpx/L}$ in their experiments.

Attempts to correlate other aspects of the clinopyroxene and melt chemistry with the $D_F^{cpx/L}$ were not successful in comparison to those involving aluminum in the crystal. Hence, our results demonstrate that the extent of aluminum incorporation into the clinopyroxene structure exerts the strongest control on the partitioning of fluorine. The correlation between $D_F^{cpx/L}$ and Al in the M1 site reproduces the measurements of this study to within 25% (relative), as shown in Figure 2b. We do not discount the possibility that more complex (multivariate) measures of major element composition (e.g.,

278 $Al^{M1} + Na^{M2}$) may correlate with $D_F^{cpx/L}$, but delay this discussion until after comparison of the results
279 of this study with previous ones. Below, we combine our results with those available in the literature to
280 investigate multivariate correlations of the fluorine partition coefficients with major element
281 compositions of clinopyroxenes and the NBO/T ratios of the melts.

282

283 **Comparison with previous studies of F partitioning between clinopyroxene and melt**

284 The results of this study are combined with those of previous experimental studies that
285 measured the partition coefficient of fluorine between quadrilateral pyroxenes and melt (Figure 3) in
286 iron- and aluminum-bearing systems. The fluorine partition coefficients published in Van den Bleeken
287 and Koga (2015) and Beyer et al. (2016) were measured on clinopyroxenes containing substantially
288 higher concentrations of the non-quadrilateral components (i.e., not Ca, Mg, Fe, and Si) than normally
289 found in igneous pyroxenes. We therefore excluded all these non-quadrilateral clinopyroxenes from
290 comparison in Figure 3 because we focus on the quadrilateral clinopyroxenes commonly found in
291 igneous rocks. We calculated the site occupancies from the published clinopyroxene compositions
292 measured in previous F partitioning experiments (Fig. 1) following the same methods as used above for
293 the experimental run products of this study.
294 The fluorine partition coefficients plotted in Figure 3 can be separated into those measured by
295 E. Hauri and colleagues (Hauri et al. 2006; O'Leary et al. 2010; Rosenthal et al. 2015) at the
296 Department of Terrestrial Magnetism, Carnegie Institute of Washington (labelled the "DTM trend" in
297 Figs. 3a and b), those analyzed by Dalou and co-workers (Dalou et al. 2012, 2014) at Woods Hole
298 Oceanographic Institute, those in the Ph.D. dissertation of Guggino (2012) at Arizona State University,
299 and ours measured at the Swedish Museum of Natural History. Most of the 63 partitioning experiments
300 were performed between 0.8 and 1.6 GPa, although a few were at pressures between 2.0 and 3.0 GPa (2

experiments in Hauri et al. 2006; 1 in Dalou et al. 2012; 7 in Rosenthal et al. 2015) and others between 0.5 and 0.1 GPa (1 in Hauri et al. 2006; 5 in Guggino 2012). The experimental temperatures of these other studies were similar to those of this study: 1000 to 1430 °C, with most in the range of 1050 to 1250 °C. The oxygen fugacities of reported experiments in the previously published studies were also similar to those of this investigation, from approximately 2 log units below the fayalite-quartz-magnetite buffer to 2 log units above. These experimental conditions allow us to make direct comparisons between the partitioning behaviour of F between clinopyroxene and melt in these different studies and to extend our results to a wider range of compositions, pressures, and temperatures (e.g., Fig. 1).

With the exception of our high oxygen fugacity experiments and the results of Dalou et al. (2014), data from each ion probe form linear or sub-linear arrays with positive slopes when $D_F^{cpx/L}$ is plotted versus Al^{IV} in Figure 3a. The partition coefficients on the DTM trend are consistently below those measured in other laboratories and display a significantly lower slope when plotting $D_F^{cpx/L}$ versus Al^{IV} (Fig. 3a). However, the data cluster tightly around the best-fit linear relationship, unlike what is seen for the data of Dalou et al. (2012), Guggino (2012), and this study (Fig. 3a). The linear fit to Guggino's results is similar to the fit to our measurements (Fig.3a), and although the Dalou et al. (2012) results are offset to lower values, their correlation line is subparallel to our and Guggino's correlations. All of these three studies (Dalou et al. 2012; Guggino 2012; and ours) as well as the measurement in Dalou et al. (2014) for a clinopyroxene with Al^{IV} less than 0.19 can be fit with a single straight line, the "others $Al^{IV} < 0.19$" trend in Figure 3a. Due to the large scatter about the line the fit is quite poor (Fig. 3a), however this fit can reproduce the measured partition coefficients from these studies to within a factor of 2*x*. Including the high oxygen fugacity, high Al^{IV} clinopyroxenes in this

study require a logarithmic fit to account for all the measurements, as seen in Figure 3a. The fit of the regression line to the data is poor, but still predicts the measured $D_F^{cpx/L}$ to within ~ 2*x*.

If instead $D_F^{cpx/L}$ is plotted as a function of Al^{M1}, each study describes a more clearly defined linear trend (Fig. 3b). The slope of the regression is greatest for the results of Guggino (2012), then decreases to the similar slopes of our work and that defined by 4 of Dalou et al.'s (2012) five measurements (the one measurement from Dalou et al. at high Al^{M1} and a low $D_F^{cpx/L}$ was not used for fitting). Note that the two measurements of Dalou et al. (2014) create a trend consistent with the fit to the Dalou et al. (2012) results. The combined measurements from the Department of Terrestrial Magnetism form a linear trend (Fig. 3b), but three individual subtrends within the data can be seen: Hauri et al.'s (2006) measurements on the run products of Gaetani and Grove (1998), O'Leary et al. (2010), and Rosenthal et al. (2015). The other studies included in Hauri et al. (2006) were not considered sufficiently numerous for the construction of regression lines (Fig. 3b).

Binary relationships between the fluorine partition coefficient and site occupancies of sodium in the M2 site (Fig. 3c), the Mg number (Fig. 3d), and the ferric iron in the M1 site (Fig. 3e) were investigated. No single trend that included all of the different studies was found. Investigation of the relationship between the F partition coefficient and the NBO/T ratio failed to produce a linear relationship (not shown), but when the partition coefficient is plotted as a function of the inverse of the NBO/T ratio, or the T/NBO ratio, a linear correlation is observed (Fig. 3f), although three measurements from anhydrous experiments in this study deviate significantly from the trend. We note that re-evaluation of these apparently anomalous experiments did not provide any reason to discard these data, so we retained them in our study.

Both Guggino (2012) and Dalou et al. (2014) also found relationships between NBO/T and the fluorine partition coefficient. Guggino (2012) discussed the observation that decreasing NBO/T (or

increasing T/NBO) values generally correlate with increasing SiO_2 in the melt. Therefore following Guggino (2012), and using Le Chatelier's rule, any reaction for the incorporation of F into a crystal that includes SiO_2 as a reactant should result in an increase of the F partition coefficient with decreasing NBO/T (increasing T/NBO or, in general, SiO_2 in the melt). Thus, a positive correlation between the F partition coefficient and T/NBO should be expected, as seen in Figure 3f.

Correlation of the F partition coefficient with multiple compositional and intensive parameters

The linear correlations observed between the F partition coefficient and both the Al^{M1} and T/NBO ratio (Fig. 3) suggest that F partitioning might be correlated with a combination of these major-element characteristics of the clinopyroxenes and melts. This hypothesis was tested using the R Project software (https://www.r-project.org/). Although the resulting correlation only displays an r^2 value of 0.4193 (Fig. 4a), addition of the pressure and temperature of the experiments to the fit increases the r^2 to 0.6060 (Fig. 4b) and yields the following empirical equation:

$$\ln(D_F^{cpx/L}) = (0.2298 \pm 0.04847)(T/NBO) - (1.029 \pm 0.8045)(Al^{M1}) - (3889 \pm 1803)(1/T) - (0.5472 \pm 0.1084)(P) + 0.5871 \pm 1.304 \quad , \quad (2)$$

where each uncertainty is 1 standard error in the fit (as calculated by the R-project software), T is in Kelvins and P is in GPa. The number of digits exceeds the precision of the measurements, but the digits are retained to minimize rounding errors in the calculation of the partition coefficient. This fit reproduces the measured partition coefficients of 81% of the data to within 25 relative percent (Fig. 4b), however the uncertainties in the fitted parameters of Equation 2 are significant. We interpret these large uncertainties to indicate that even though this was the best fit found between major element compositional parameters and the fluorine partition coefficient, this empirical fit is not robust (see discussion below).

This is the peer-reviewed, final accepted version for American Mineralogist, published by the Mineralogical Society of America.
The published version is subject to change. Cite as Authors (Year) Title. American Mineralogist, in press.
DOI: https://doi.org/10.2138/am-2021-7868. http://www.minsocam.org/

Attempts to fit other multiple compositional parameters of the clinopyroxene and melt compositions (including the melt water concentration) with the measured fluorine partition coefficients of all the studies did not result in better correlations than Equation 2. For example, although Mosenfelder and Rossman (2013) found a correlation between the F concentrations in clinopyroxene and $Na + K + Al^{IV}$ ($r^2 = 0.92$), our correlation between the F partition coefficients and these major element characteristics of the clinopyroxenes only produced a correlation coefficient of $r^2 = 0.015$. Combinations of multiple compositional parameters of the crystals and the melts combined with pressure and temperature failed to produce any correlations with r^2 values superior to those reported in Figure 4b. In most cases the r^2 values were between 0.4 and 0.5. Importantly, no effect of water concentration in the melt on fluorine partitioning was observed.

Toward a general model for the prediction of the partitioning of fluorine between clinopyroxene and melt

Figure 4b demonstrates that the inverse of the NBO/T ratio combined with the Al^{M1} value, temperature, and pressure can be used to estimate the fluorine partition coefficient between quadrilateral clinopyroxenes and melts. This empirical correlation (Eqn. 2) provides the best relationship for all the measured fluorine partition coefficients found. Despite the limitations of Equation 2 (see above), given the necessary input parameters, the partitioning behavior of fluorine between quadrilateral clinopyroxenes and melt can be predicted. The predictions are best for partition coefficient values of 0.12 or less (Fig. 4b). However, the poor quality of the fit shown in Equation 2 (i.e. low r^2 combined with large uncertainties in the fitted values) is probably due to the challenge of analyzing low concentrations of fluorine in crystals and by the combination of data from multiple laboratories.

The observation that each $D_F^{cpx/L}$ data set defines a linear trend when plotted as a function of either Al^{IV} or Al^{M1} (Figs. 3a and 3b) is interpreted to be due to differing analytical techniques. Rose-Koga et al. (2020) demonstrated the precision and accuracy of ion microprobe analyses of silicate glasses using analyses at Woods Hole. However, we are unaware of similar studies on clinopyroxene with low F concentrations and suggest that the differences in partition coefficients measured at different laboratories seen in Figure 3 result from the analyses of clinopyroxene, not the quenched glass, and may possibly be due to differing matrix effects of the reference glasses and the clinopyroxene crystals. These results suggest that caution should be used when combining partition coefficients measured on one ion microprobe using a specific set of standards with samples measured on a different machine with different standards.

Fluorine partitioning between melt and olivine, orthopyroxene, and plagioclase

The paucity of analyses for the other phases in the run products does not allow for a detailed investigation of the relationships between mineral composition and the fluorine partition coefficients. However there are consistent patterns between our few crystal-melt partitioning measurements on other phases and fluorine partitioning between clinopyroxene and melt. The $D_F^{crystal/L}$ between both olivine and melt and orthopyroxene and melt are similar to the minimum value measured between clinopyroxene and melt, ~ 0.05 to 0.08 (Fig. 5), whereas the values of $D_F^{crystal/L}$ between plagioclase and melt are lower, 0.04-0.05 (Fig. 5). These results are consistent with previously measured fluorine partition coefficients between melt and olivine or orthopyroxene in experiments, but the four new measurements for plagioclase partitioning are lower than the few values available in the literature (Fig. 5; Dalou et al. 2012; Guggino 2012), but only by a factor of ~1/2. The extent to which the variations seen in the measured fluorine partition coefficients between these minerals and melts are affected by differences in analytical techniques, as suggested above for clinopyroxene, remains unknown.

This is the peer-reviewed, final accepted version for American Mineralogist, published by the Mineralogical Society of America.
The published version is subject to change. Cite as Authors (Year) Title. American Mineralogist, in press.
DOI: https://doi.org/10.2138/am-2021-7868. http://www.minsocam.org/

Chlorine partitioning between crystals and melts

The mineral-melt chlorine partition coefficients measured in this study are compared in Figure 5 with previous measurements of $D_{Cl}^{crystal/L}$ (Dalou et al. 2012, 2014). The $D_{Cl}^{crystal/L}$ measurements of this study are considered maximum values because the chlorine concentrations measured in the crystals were very close to those measured in Herasil® glass. Nevertheless, the values we measured are similar to those in the literature for the ferromagnesian phases. On the other hand, the $D_{Cl}^{crystal/L}$ for plagioclase is about an order of magnitude greater than the value found by Dalou et al. (2012). These few results demonstrate a pressing need for more high-quality analyses of chlorine partitioning between common magmatic minerals and melts.

Comparison of halogen partition coefficients with those of other volatile elements

Figure 5 also compares the halogen partitioning measurements of this study and others with partitioning of hydrogen (or water), carbon, and total sulfur. All of these elements in almost all of the crystals studied are incompatible, although the fluorine partition coefficient can slightly exceed 1 in amphibole (Fig. 5). There is a general trend of increasing compatibility from olivine, orthopyroxene, clinopyroxene and amphibole, then a decrease for plagioclase for most of the volatile elements (Fig. 5). The exception is carbon, for which the data are limited. The partitioning behavior in the different minerals in Figure 5 is due to their different compositions and structures, which influence the partition coefficients. However, as shown above for fluorine partitioning between clinopyroxene and melt, a full understanding of those controls will require many more experimental measurements of partition coefficients.

IMPLICATIONS

The linear correlations of the fluorine partition coefficient between clinopyroxene and melt with the Al site occupancies and T/NBO, temperature, and pressure (Figs. 3, 4) allow researchers to use the

438 measured concentrations of F in common igneous quadrilateral clinopyroxenes to determine the
439 concentrations of F in coexisting melts. This correlation extends our ability to investigate pre-eruption
440 volatile concentrations in magmas to clinopyroxene-bearing samples that may have few, or no, melt
441 inclusions. Any zoning of F observed in natural clinopyroxenes has the potential to be used to infer
442 volatile evolution and provide additional constraints on pre-eruptive behavior of magmatic systems,
443 e.g., discerning degassing trends or recharging of the system with more volatile-rich magmas. More
444 specifically, the application of halogen partition coefficients to minerals will allow us to better
445 constrain the environmental impacts of ancient volcanic eruptions and hopefully to determine if
446 halogen-rich eruptions are due to high halogen concentrations in the magmatic source regions (e.g.
447 Broadley et al. 2018) or assimilation of halogen-enriched crustal rocks (e.g., Black et al. 2012).

448 Despite the correlation found between Al^{M1}, T/NBO, 1/T, P, and $D_F^{cpx/L}$ (Eqn. 2, Fig. 4b), a very
449 important caveat remains. As shown in Figure 3, we suggest that the different relationships between the
450 partition coefficient and the major element chemistries of the clinopyroxene and the melt are a function
451 of the analytical techniques used to measure F in clinopyroxene. Thus, until we fully understand the
452 source of the differences seen in Figure 3 there can be no "universal" relationship for $D_F^{cpx/L}$ and major
453 element compositions of the melt and clinopyroxene that provides an accuracy better than ~ 25%
454 (relative) as seen in Figure 4b. Instead, the best choice appears to be that of using the relationship
455 between Al^{M1} and $D_F^{cpx/L}$ determined on the same ion microprobe using the same standards as used to
456 measure the partition coefficient. Although this is not an ideal situation, each set of experimentally
457 measured partition coefficients appears internally consistent and can be combined with analyses of
458 samples using the same protocol to provide useful constraints on the storage and transport of fluorine in
459 magmatic systems.

460

Acknowledgements

Funding for this study was provided by NSERC Discovery Grants to D.R.B, by the Research Council of Norway Yngeforsktalenter project "MAPLES" (project number 301096) to S.C,, and by the Italian Ministry of Research (PRIN 20178LPCP) to A.M. and A.D.M. We also thank the associate Editor D. Harlov and the official reviewers R. Hervig (who encouraged us to investigate the relationship be F partitioning and the electrostatic calculations of Smyth, 1989) and B. Joachim-Mrosko, as well as K. Koga and E. Rose-Koga whose comments on an early version of the manuscript substantially improved our understanding and presentation.

References

Adam, J., and Green, T.H. (1994) The effects of pressure and temperature on the partitioning of Ti, Sr and REE between amphibole, clinopyroxene and basanitic melts. Chemical Geology, 117, 219-233.

Baker, D.R. (2004) Piston cylinder calibration at 400 to 500 MPa: a comparison of using water solubility in albite melt and NaCl melting. American Mineralogist, 89, 1553–1556.

Baker, D.R. (2008) The fidelity of melt inclusions as records of melt composition. Contributions to Mineralogy and Petrology, 157, 377–395.

Baker, D.R., and Eggler, D.H. (1987) Compositions of anhydrous and hydrous melts coexisting with plagioclase, augite, and olivine or low-Ca pyroxene from 1 atm. to 8 kbar: application to the Aleutian volcanic center of Atka. American Mineralogist, 72, 12–28.

Bénard, A., Koga, K.T., Shimizu, N., Kendrick, M.A., Ionov, D.A., Nebel, O., and Arculus, R.J. (2017) Chlorine and fluorine partition coefficients and abundances in sub-arc mantle xenoliths (Kamchatka, Russia): implications for melt generation and volatile recycling processes in subduction zones. Geochimica et Cosmochimica Acta, 199, 324–350.

Beyer, C., Klemme, S., Wiedenbeck, M., Stracke, A., and Vollmer, C. (2012) Fluorine in nominally fluorine-free mantle minerals: experimental partitioning of F between olivine, orthopyroxene and silicate melts with implications for magmatic processes. Earth and Planetary Science Letters, 337–338, 1–9.

Black, B.A., Elkins-Tanton, L.T., Rowe, M.C., and Peate, I.U. (2012) Magnitude and consequences of volatile release from the Siberian Traps. Earth and Planetary Science Letters, 317-318, 263-373.

Bond, D.P.G., and Wignall, P.B. (2014) Large igneous provinces and mass extinctions: an update. Geological Society of America Special Paper, 505, SPE505-02.

Broadley, M.W., Barry, P.H., Ballentine, C.J. *et al.* (2018) End-Permian extinction amplified by plume-induced release of recycled lithospheric volatiles. Nature Geosciences, 11**,** 682–687. https://doi-org.ezproxy.uio.no/10.1038/s41561-018-0215-4

Callegaro, S., Geraki, K., Marzoli, A., De Min, A., Maneta, V., and Baker, D.R. (2020) The quintet completed: The partitioning of sulfur between nominally volatile-free minerals and silicate melts. American Mineralogist, 105, 697-707.

Cannatelli, C., Doherty, A. L., Esposito, R., Lima, A., and Vivo, B. De (2016) Understanding a volcano through a droplet: A melt inclusion approach. Journal of Geochemical Exploration, 171, 4–19.

D'Alessandro, W. (2006) Human fluorosis related to volcanic activity: a review. Environmental Toxicology, 10, 21-30.

Dalou, C., Le Losq, C., Mysen, B.O., and Cody G.D. (2015) Solubility and solution mechanisms of chlorine and fluorine in aluminosilicate melts at high pressure and high temperature. American Mineralogist, 100, 2272-2283.

Dalou, C., Koga, K.T., Shimizu, N., Boulon, J., and Devidal, J-L. (2012) Experimental determination of F and Cl partitioning between lherzolite and basaltic melt. Contributions to Mineralogy and Petrology, 163, 591–609.

Dalou, C., Koga, K.T., Le Voyer, M., and Shimizu, N. (2014) Contrasting partition behavior of F and Cl during hydrous mantle melting: Implications for Cl/F in arc magmas. Progress in Earth and Planetary Sciences, 1, 26, 10.1186/s40645-014-0026-1.

Devine, J.D., Sigurdsson, H., Davis, A.N., and Self, S. (1984) Estimates of sulfur and chlorine yield to the atmosphere from volcanic eruptions and potential climatic effects. Journal of Geophysical Research, 89, 6309-6325.

Edmonds, M. (2008) New geochemical insights into volcanic degassing. Philosophical Transactions of the Royal Society A: Mathematical, Physical and Engineering Sciences, 366, 4559–4579.

Gaetani G.A., and Grove, T.L. (1998) The influence of water on melting of mantle peridotite. Contributions to Mineralogy and Petrology, 131, 323-346.

Green, T.H., Blundy, J.D., Adam, J., and Yaxley, G.M. (2000) SIMS determination of trace element partition coefficients between garnet, clinopyroxene and hydrous basaltic liquids at 2 – 7.5 GPa and 1080-1200 ºC. Lithos, 53, 165-187.

Guggino, S.N. (2012) Fluorine partitioning between nominally anhydrous minerals (olivine, clinopyroxene, and plagioclase) and silicate melt using secondary ion mass spectrometry and newly synthesized basaltic fluorine microanalytical glass standards. 249 p. Ph.D. Thesis, Arizona State University, Tempe.

Hamada, M., Ushioda, M., Fujii, T., and Takahashi, E. (2013) Hydrogen concentration in plagioclase as a hygrometer of arc basaltic melts: Approaches from melt inclusion analyses and hydrous melting experiments. Earth and Planetary Science Letters, 365, 253–262.

Hansell, A.L., Horwell, C.J., and Oppenheimer, C. (2006) The health hazard of volcanoes and geothermal areas. Occupational & Environmental Medicine, 64, 149-156.

Harlov, D. and Aravnovich, L. , Eds. (2018) The Role of Halogens in Terrestrial and Extraterrestrial Geochemical Processes, 1030 p. Springer Geochemistry, Springer International Publishing, Cham.

Hauri, E.H., Gaetani, G.A., and Green, T.H. (2006) Partitioning of water during melting of the Earth's upper mantle at H_2O-undersaturated conditions. Earth and Planetary Science Letters, 248, 715–734.

Joachim, B., Pawley, A., Lyon, I.C., Marquardt, K., Henkel, T., Clay, P.L., Ruzié, L., Burgess, R., and Ballentine, C.J. (2015) Experimental partitioning of F and Cl between olivine, orthopyroxene and silicate melt at Earth's mantle conditions. Chemical Geology, 416, 65-78.

Jochum, K. P., Stoll, B., Herwig, K., Willbold, M., Hofmann, A.W., Amini, M., Aarburg, S., Abouchami, W., Hellebrand, E., Mocek, B., and others (2006) MPI-DING reference glasses for in situ microanalysis: New reference values for element concentrations and isotope ratios, Geochemistry, Geophysics, Geosystems, 7, Q02008.

Johnson, M.C., Anderson, A.T. Jr., and Rutherford, M.J. (1994) Pre-eruptive volatile contents of magmas. In M.R. Carroll and J.R. Holloway, Eds., Volatiles in Magmas. Reviews in Mineralogy, 30, 281–330.

Kovalenko, V. I., Hervig, R. L., and Sheridan, M. F. (1988) Ion microprobe analyses of trace elements in anorthoclase, hedenbergite, aenigmatite, quartz, apatite and glass in pantellerite: Evidence for high water contents in pantellerite melts. American Mineralogist, 73, 1038-1045.

Kusebauch, C., John, T., Whitehouse, M.J., Klemme, S., and Putnis, A. (2015) Distribution of halogens between fluid and apatite during fluid-mediated replacement processes. Geochimica et Cosmochimica Acta, 170, 225-246.

La Tourrette, T., Hervig, R.L., and Holloway, J.R. (1995) Trace element partitioning between amphibole, phlogopite, and basanite melt. Earth and Planetary Science Letters, 135, 13-30.

Mosenfelder, J.L., and Rossman, G.R. (2013) Analysis of hydrogen and fluorine in pyroxenes: II. Clinopyroxene. American Mineralogist, 98, 1042-1054.

Mysen, B., and Richet, P. (2019) Silicate melts and glasses, 2nd edition. 708 p. Elsevier, Amsterdam.

559 Mysen, B.O., Cody, G.D., and Smith, A. (2004) Solubility mechanisms of fluorine in peralkaline and
560 meta-aluminous silicate glasses and in melts to magmatic temperatures. Geochimica et
561 Cosmochimica Acta, 68, 2745–2769.

562 O'Leary, J.A., Gaetani, G.A., and Hauri, E.H. (2010) The effect of tetrahedral Al^{3+} on the partitioning of
563 water between clinopyroxene and silicate melt. Earth and Planetary Science Letters, 297, 111-
564 120.

565 Robock, A. (2013) The latest on volcanic eruptions and climate. EOS, 94, 305–307.

566 Rose-Koga E.F., Koga K.T., Devidal, J.-L., Shimizu, N., Le Voyer, M., Dalou, C., and Döbeli, M.
567 (2020) In-situ measurements of magmatic volatile elements, F, S, and Cl, by electron microprobe,
568 secondary ion mass spectrometry, and heavy ion elastic recoil detection analysis. American
569 Mineralogist, 105, 616-626.

570 Rosenthal, A., Hauri, E.H., and Hirschmann, M.M. (2015) Experimental determination of C, F, and H
571 partitioning between mantle minerals and carbonated basalt, CO_2/Ba and CO_2/Nb systematics of
572 partial melting, and the CO_2 contents of basaltic source regions. Earth and Planetary Science
573 Letters, 412, 77–87.

574 Schaller, T., Dingwell, D.B., Keppler, H., Knöller, W., Merwin, L., and Sebald, A. (1992) Fluorine in
575 silicate glasses: A multinuclear nuclear magnetic resonance study. Geochimica et Cosmochimica
576 Acta, 56, 701–707.

577 Self, S., Schmidt, A., and Mather, T. A. (2014) Emplacement characteristics, time scales, and volcanic
578 gas release rates of continental flood basalt eruptions on Earth. In Keller, G., and Kerr, A.C., Eds.,
579 Volcanism, Impacts, and Mass Extinctions: Causes and Effects: Geological Society of America
580 Special Paper, 505, 319–337.

581 Smyth, J.R. (1989) Electrostatic characterization of oxygen sites in minerals. Geochimica et
582 Cosmochimica Acta, 53, 1101-1110.

583 Symonds, R.B., Rose, W.I., Bluth, G.S., and Gerlach, T.M. (1994) Volcanic gas studies, methods,
584 results and applications. In M.R. Carroll and J.R. Holloway, Eds., Volatiles in Magmas. Reviews
585 in Mineralogy, 30, 1–66.

586 Tonarini, S., Pennisi, M., Adorni-Braccesi, A., Dini, A., Ferrara, G., Gonfiantini, R., Wiedenbeck, M.,
587 and Gröning, M. (2003) Intercomparison of boron isotope and concentration measurements. Part

I: Selection, preparation and homogeneity tests of the intercomparison materials. Geostandards Newsletter: The Journal of Geostandards and Geoanalysis, 27, 21-39.

Urann, B.M., Le Roux, V., Hammond, K., Marschall, H.R., Lee, C.T.A. and Monteleone, B.D. (2017) Fluorine and chlorine in mantle minerals and the halogen budget of the Earth's mantle. Contributions to Mineralogy and Petrology, 172, 1–17.

Van den Bleeken, G., and Koga, K.T. (2015) Experimentally determined distribution of fluorine and chlorine upon hydrous slab melting, and implications for F-Cl cycling through subduction zones. Geochimica et Cosmochimica Acta, 171, 353–373.

Webster, J. D., Baker, D. R., and Aiuppa, A. (2018) Halogens in mafic and intermediate-silica content magmas. In D.Harlov and L. Aranovich Eds., The Role of Halogens in Terrestrial and Extraterrestrial Geochemical Processes, Springer Geochemistry, Springer International Publishing, Cham. https://doi.org/10.1007/978-3-319-61667-4_6

Wignall, P.B. (2001) Large igneous provinces and mass extinctions. Earth Science Reviews, 53, 1–33.

Zeng, Q., and Stebbins, J.F. (2000) Fluoride sites in aluminosilicate glasses: High-resolution ^{19}F NMR results. American Mineralogist, 85, 863–867.

This is the peer-reviewed, final accepted version for American Mineralogist, published by the Mineralogical Society of America.
The published version is subject to change. Cite as Authors (Year) Title. American Mineralogist, in press.
DOI: https://doi.org/10.2138/am-2021-7868. http://www.minsocam.org/

Figure captions

Figure 1 Compositions of clinopyroxenes produced in this study and previously published studies on fluorine partitioning between clinopyroxene and melt (Hauri et al. 2006, that included samples from Adam and Green 1994; Gaetani and Grove 1998; and Green et al. 2000; O'Leary et al. 2010; Dalou et al. 2012, 2014; Guggino 2012; Rosenthal et al. 2015). a) Q versus J plot following Morimoto et al. (1988) where Q = Ca + Fe^{2+} + Mg and J = 2 Na. b) pyroxene quadrilateral plot where En is the enstatite component, Wo is the wollastonite component, and Fs is the ferrosilite component calculated using the total iron in the clinopyroxene. (color online)

Figure 2 Relationships between D_F and clinopyroxene compositions or melt composition measured in this study. a) D_F versus Al^{IV} (site occupancy of aluminum in the tetrahedral site in clinopyroxene, apfu). b) D_F versus Al^{M1} (site occupancy of aluminum in the M1 octahedral site in clinopyroxene, apfu). c) D_F versus Na^{M2} (site occupancy of sodium in the M2 distorted octahedral site in clinopyroxene, apfu). d) D_F versus molar Mg/(Mg+Fe^{total}) in the clinopyroxene. e) D_F versus Fe^{3+} site occupancy in the M1 octahedral site, as calculated from clinopyroxene stoichiometry and charge balance. f) D_F versus the ratio of non-bridging oxygens to tetrahedral cations in the anhydrous melt (NBO/T).

Figure 3 Relationships between the D_F and quadrilateral clinopyroxene compositions measured in this and other experimental studies of fluorine partitioning between quadrilateral clinopyroxenes and silicate melts (Hauri et al. 2006, that included samples from Adam and Green 1994; Gaetani and Grove 1998; and Green et al. 2000; O'Leary et al. 2010; Dalou et al. 2012, 2014; Guggino 2012; Rosenthal et al. 2015). a) D_F versus Al^{IV} (mole fraction of aluminum in the tetrahedral site in clinopyroxene, apfu). b) D_F versus Al^{M1} (mole fraction of aluminum in the M1 octahedral site in clinopyroxene, apfu). c) D_F versus Na^{M2} (mole fraction of sodium in the M2 site in clinopyroxene, apfu). d) D_F versus molar Mg/(Mg+Fe^{total}) in the clinopyroxene. e) D_F versus Fe^{3+} site occupancy in the M1 octahedral site, as calculated from clinopyroxene stoichiometry and charge balance. f) D_F versus the inverse of the ratio of non-bridging oxygens to tetrahedral cations in the anhydrous melt (NBO/T), or the T/NBO ratio. The "DTM trend" is composed of partition coefficients from various studies that were all analyzed at the Department of Terrestrial Magnetism. (color online)

Figure 4 The calculated versus measured partitioning of fluorine between quadrilateral clinopyroxene and melt. a) Model using only Al^{M1} (apfu) of the quadrilateral clinopyroxenes and T/NBO of the coexisting melts. b) Model using Al^{M1} (apfu) of the quadrilateral clinopyroxenes,

T/NBO of the coexisting melts, pressures, and temperatures of the experiments. The data and symbols are the same as in Figure 3. The temperature in the fit is in K and the pressure in Gpa. (color online)

Figure 5 Partition coefficients of F and Cl between crystals and melts measured in this (with their 1-sigma standard deviations, which are often smaller than the symbols.) compared to the range of values measured in previous studies, including those investigating non-quadrilateral clinopyroxenes and natural samples (Kovalenko et al. 1988; LaTourette et al. 1995; Hauri et al. 2006; O'Leary et al. 2010; Dalou et al. 2012, 2014; Guggino 2012; Beyer et al. 2012; 2016; Joachim et al. 2015; Rosenthal et al. 2015; Van den Bleeken and Koga 2015; Bénard et al. 2017; Lloyd et al. 2016). Also plotted are the range of partition coefficients for carbon, hydrogen as water (Hauri et al. 2006; Hamada et al. 2013; Rosenthal et al. 2015; Lloyd et al. 2016), and total sulfur (Callegaro et al. 2020). Note that the Cl concentrations measured in the crystals of this study are near background levels and therefore the partition coefficients should be considered maximum values; see text for more discussion. (color online)

Table 1: Run conditions, F and Cl concentrations (mean and standard deviation), and their partition coefficients

Experiment	P (GPa)	T (°C)[a]	Duration (h)[b]	ΔFMQ[c]	phase	H_2O[d] (wt %)	n[e]	F (ppm)	D-F[f]	Cl (ppm)	D-Cl[g]
Basaltic starting material MORB											
DRB2012-36	1.0	1350/1240	2/20.1	-2	glass	n.a.[h]	11	264.5 (2.0)[i]		135.6 (11.4)	
					cpx		10	62.9 (9.7)	0.238 (0.037)	1.8 (0.5)	0.013 (0.004)
DRB2012-38	1.2	1350/1240	2/20	-2	glass	n.a.	16	284.8 (3.7)		139.9 (3.9)	
					cpx		13	81.5 (6.8)	0.286 (0.024)	1.3 (0.3)	0.010 (0.002)
CS2014-13	1.0	1350/1240	2/24	1.8	glass	n.a.	9	213.4 (7.8)		89.9 (7.4)	
					cpx		11	38.6 (4.2)	0.181 (0.021)	1.2 (0.6)	0.013 (0.006)
DRB2015-1	1.0	1150/1060	2/24	1.5	glass	7.6 (0.9)	14	251.9 (23.8)		106.2 (15.3)	
					cpx		8	22.4 (8.1)	0.089 (0.033)	0.9 (0.2)	0.008 (0.003)
Basaltic starting material AN-31											
DRB2012-29	0.8	1350/1240	2/24	-2	glass	n.a.	4	439.0 (2.4)		410.9 (5.1)	
					opx		4	25.3 (0.7)	0.058 (0.002)	1.5 (0)	0.004
					oliv		5	20.3 (1.9)	0.046 (0.005)	1.4 (0.1)	0.003
DRB2012-35	1.0	1350/1240	2/20.1	-2	glass	n.a.	10	495.3 (4.8)		503.5 (7.0)	
					cpx		8	56.1 (6.4)		2.2 (1.7)	0.004 (0.003)
DRB2012-37	1.2	1350/1240	2/20	-2	glass	n.a.	9	505.4 (6.0)		456.8 (14.7)	
					cpx		8	70.1 (5.6)	0.139 (0.011)	1.2 (0.1)	0.003
CS2014-14	1.0	1350/1240	2/24	1.7	glass	n.a.	8	426.2 (15.3)	0.73	503.7 (1.2)	
					opx		17	34.1 (2.5)	0.080 (0.007)	0.8 (0.1)	0.001
Andesitic starting material AT-29D											
CS2014-9	0.8	1300/1160	2/24	-2	glass	n.a.	14	538.7 (15.8)		111.7 (6.6)	
					cpx		5	62.4 (3.1)	0.116 (0.007)	2.9 (0.9)	0.026 (0.008)
					plag		1	21.8 (0.7)	0.041 (0.002)	1.600	0.014
CS2014-5	0.8	1300/1140	1/24	-2	glass	n.a.	5	527.3 (17.0)		138.1 (38.1)	
					cpx		5	48.5 (5.9)	0.092 (0.012)	2.4 (1,6)	0.017 (0.013)
					plag		6	17.8 (5.4)	0.034 (0.010)	1.2 (0.5)	0.009 (0.005)
CS2014-3	0.8	1300/1118	1/24	-2	glass	n.a.	6	451.4 (24.4)		92.0 (15.9)	
					cpx		5	50.7 (2.3)	0.112 (0.008)	2.3 (0.9)	0.025 (0.011)
					plag		3	16.1 (2.0)	0.036 (0.005)	0.9 (0)	0.010 (0.002)
DRB2015-2	1.0	1150/1060	2/24	1.5	glass	6.3 (0.3)	6	319.8 (0.9)		53.7 (0.4)	
					cpx		11	35.6 (4.0)	0.111 (0.012)	0.7 (0)	0.014 (0.001)
CS2014-19	0.8	1150/1000	2/24	0.9	glass	11.2 (0.5)	5	337.6 (12.1)		51.4 (1.1)	
					cpx		8	60.1 (3.9)	0.178 (0.013)	2.1 (1.4)	0.040 (0.026)
Dacitic starting material AT-150											
CS2014-31	0.8	1150/1000	2/24	-2	glass	1.1 (0.3)	8	399.1 (36.1)		158.6 (35.3)	
					cpx		8	38.6 (9.9)	0.012 (0.007)	3.2 (2.8)	0.020 (0.018)
					plag		10	19.7 (7.5)	0.049 (0.019)	1.9 (1.1)	0.012 (0.007)
CS2014-20	0.8	1150/1000	2/24	1.1	glass	5.7 (0.8)	8	212.3 (8.3)		115.5 (97.2)	
					cpx		7	48.9 (2.7)	0.230 (0.015)	1.2 (0.1)	0.011 (0.009)

[a]The high temperature step of the experiment followed by the low temperature step

[b]The duration of the high temperature step followed by the duration of the low temperature step in hours

[c]The oxygen fugacity of the experiment relative to the fayalite-magnetite-quartz (FMQ buffer); see text for discussion

[d]Water concentration in quenched glasses from hydrous experiments measured by Raman spectrocopy as reported in Callegaro et al. (2020), n.a. = not analyzed

[e]Number of ion microprobe analyses for fluorine and chlorine in the indicated phase. Note that the Cl concentrations are near, or at, background levels in the cryst

[f]Crystal-melt partition coefficient of fluorine determined by dividing the fluorine measured in the crystal by the fluorine measured in the glass

[g]Crystal-melt partition coefficient of chlorine determined by dividing the chlorine measured in the crystal by the chlorine measured in the glass

[h]n.a. -- not analyzed; these experiments are nominally anhydrous

[i]Mean concentration followed by 1 standard deviation in parentheses

Table 1: Run conditions, F and Cl concentrations (mean and standard dev

Experiment	P (GPa)	T (°C)[a]	Duration (h)[b]	ΔFMQ[c]	phase	H_2O[d] (wt %)	n[e]
Basaltic starting material MORB							
DRB2012-36	1.0	1350/1240	2/20.1	-2	glass	n.a.[h]	11
					cpx		10
DRB2012-38	1.2	1350/1240	2/20	-2	glass	n.a.	16
					cpx		13
CS2014-13	1.0	1350/1240	2/24	1.8	glass	n.a.	9
					cpx		11
DRB2015-1	1.0	1150/1060	2/24	1.5	glass	7.6 (0.9)	14
					cpx		8
Basaltic starting material AN-31							
DRB2012-29	0.8	1350/1240	2/24	-2	glass	n.a.	4
					opx		4
					oliv		5
DRB2012-35	1.0	1350/1240	2/20.1	-2	glass	n.a.	10
					cpx		8
DRB2012-37	1.2	1350/1240	2/20	-2	glass	n.a.	9
					cpx		8
CS2014-14	1.0	1350/1240	2/24	1.7	glass	n.a.	8
					opx		17
Andesitic starting material AT-29D							
CS2014-9	0.8	1300/1160	2/24	-2	glass	n.a.	14
					cpx		5
					plag		1
CS2014-5	0.8	1300/1140	1/24	-2	glass	n.a.	5
					cpx		5
					plag		6
CS2014-3	0.8	1300/1118	1/24	-2	glass	n.a.	6
					cpx		5
					plag		3
DRB2015-2	1.0	1150/1060	2/24	1.5	glass	6.3 (0.3)	6
					cpx		11
CS2014-19	0.8	1150/1000	2/24	0.9	glass	11.2 (0.5)	5
					cpx		8
Dacitic starting material AT-150							
CS2014-31	0.8	1150/1000	2/24	-2	glass	1.1 (0.3)	8
					cpx		8
					plag		10
CS2014-20	0.8	1150/1000	2/24	1.1	glass	5.7 (0.8)	8
					cpx		7

[a]The high temperature step of the experiment followed by the low temperature step

[b]The duration of the high temperature step followed by the duration of the low temperature step in h

[c]The oxygen fugacity of the experiment relative to the fayalite-magnetite-quartz (FMQ buffer); see t

[d]Water concentration in quenched glasses from hydrous experiments measured by Raman spectro

[e]Number of ion microprobe analyses for fluorine and chlorine in the indicated phase. Note that the

[f]Crystal-melt partition coefficient of fluorine determined by dividing the fluorine measured in the crys

[g]Crystal-melt partition coefficient of chlorine determined by dividing the chlorine measured in the cr

[h]n.a. -- not analyzed; these experiments are nominally anhydrous

[i]Mean concentration followed by 1 standard deviation in parentheses

riation), and their partition coefficients

F (ppm)	D-F[f]	Cl (ppm)	D-Cl[g]
264.5 (2.0)[i]		135.6 (11.4)	
62.9 (9.7)	0.238 (0.037)	1.8 (0.5)	0.013 (0.004)
284.8 (3.7)		139.9 (3.9)	
81.5 (6.8)	0.286 (0.024)	1.3 (0.3)	0.010 (0.002)
213.4 (7.8)		89.9 (7.4)	
38.6 (4.2)	0.181 (0.021)	1.2 (0.6)	0.013 (0.006)
251.9 (23.8)		106.2 (15.3)	
22.4 (8.1)	0.089 (0.033)	0.9 (0.2)	0.008 (0.003)
439.0 (2.4)		410.9 (5.1)	
25.3 (0.7)	0.058 (0.002)	1.5 (0)	0.004
20.3 (1.9)	0.046 (0.005)	1.4 (0.1)	0.003
495.3 (4.8)		503.5 (7.0)	
56.1 (6.4)		2.2 (1.7)	0.004 (0.003)
505.4 (6.0)		456.8 (14.7)	
70.1 (5.6)	0.139 (0.011)	1.2 (0.1)	0.003
426.2 (15.3)	0.73	503.7 (1.2)	
34.1 (2.5)	0.080 (0.007)	0.8 (0.1)	0.001
538.7 (15.8)		111.7 (6.6)	
62.4 (3.1)	0.116 (0.007)	2.9 (0.9)	0.026 (0.008)
21.8 (0.7)	0.041 (0.002)	1.600	0.014
527.3 (17.0)		138.1 (38.1)	
48.5 (5.9)	0.092 (0.012)	2.4 (1,6)	0.017 (0.013)
17.8 (5.4)	0.034 (0.010)	1.2 (0.5)	0.009 (0.005)
451.4 (24.4)		92.0 (15.9)	
50.7 (2.3)	0.112 (0.008)	2.3 (0.9)	0.025 (0.011)
16.1 (2.0)	0.036 (0.005)	0.9 (0)	0.010 (0.002)
319.8 (0.9)		53.7 (0.4)	
35.6 (4.0)	0.111 (0.012)	0.7 (0)	0.014 (0.001)
337.6 (12.1)		51.4 (1.1)	
60.1 (3.9)	0.178 (0.013)	2.1 (1.4)	0.040 (0.026)
399.1 (36.1)		158.6 (35.3)	
38.6 (9.9)	0.012 (0.007)	3.2 (2.8)	0.020 (0.018)
19.7 (7.5)	0.049 (0.019)	1.9 (1.1)	0.012 (0.007)
212.3 (8.3)		115.5 (97.2)	
48.9 (2.7)	0.230 (0.015)	1.2 (0.1)	0.011 (0.009)

hours

text for discussion

copy as reported in Callegaro et al. (2020), n.a. = not analyzed

Cl concentrations are near, or at, background levels in the crystals.

stal by the fluorine measured in the glass

ystal by the chlorine measured in the glass

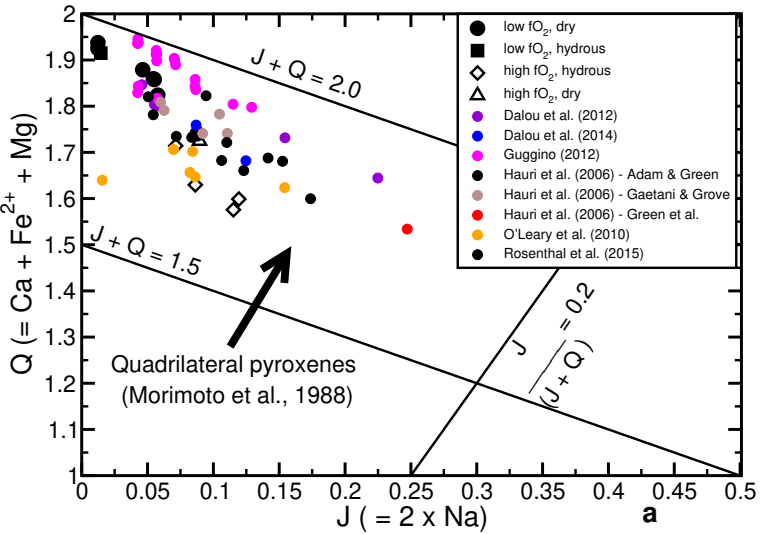
low fO2, dry
low fO2, hydrous
high fO2, hydrous
high fO2, dry
Dalou et al. (2012)
Dalou et al. (2014)
Guggino (2012)
Hauri et al. (2006) - Adam & Green
Hauri et al. (2006) - Gaetani & Grove
Hauri et al. (2006) - Green et al.
O'Leary et al. (2010)
Rosenthal et al. (2015)
J + Q = 2.0
J + Q = 1.5
J / (J + Q) = 0.2
Quadrilateral pyroxenes
(Morimoto et al., 1988)
Q (= Ca + Fe2+ + Mg)
J (= 2 x Na)
a

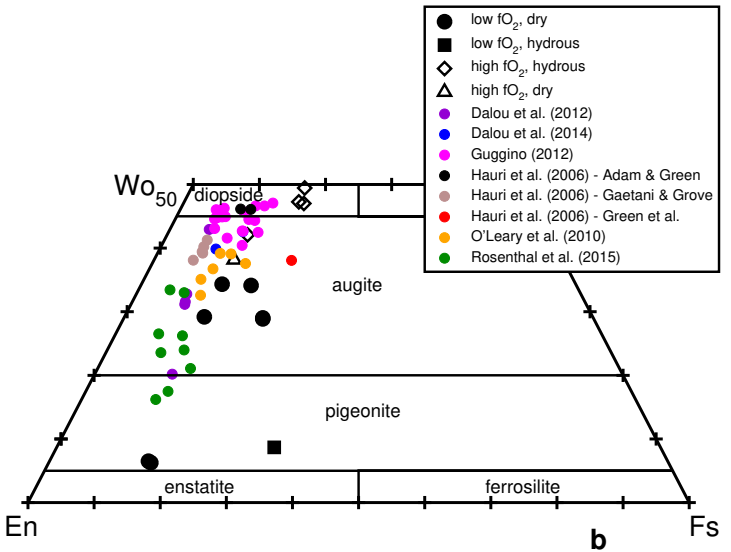
low fO2, dry
low fO2, hydrous
high fO2, hydrous
high fO2, dry
Dalou et al. (2012)
Dalou et al. (2014)
Guggino (2012)
Hauri et al. (2006) - Adam & Green
Hauri et al. (2006) - Gaetani & Grove
Hauri et al. (2006) - Green et al.
O'Leary et al. (2010)
Rosenthal et al. (2015)
Wo50
diopside
augite
pigeonite
enstatite
ferrosilite
En
Fs
b

Figure 1

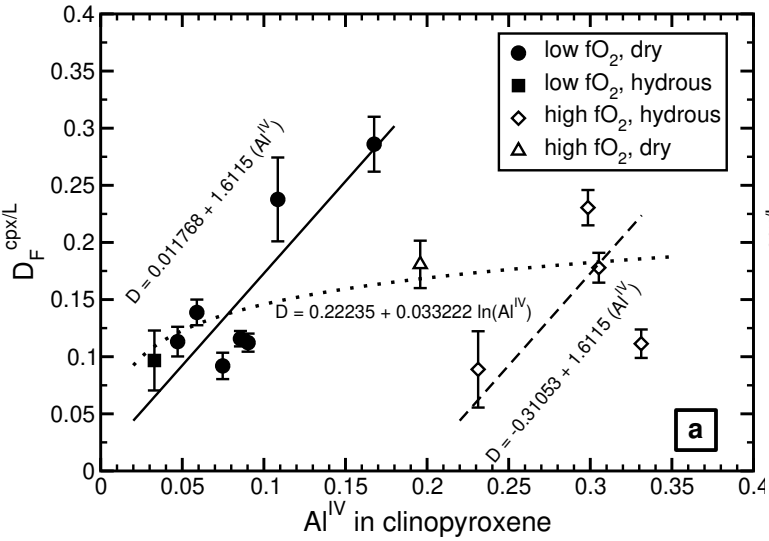
low fO2, dry
low fO2, hydrous
high fO2, hydrous
high fO2, dry
D = 0.011768 + 1.6115 (AlIV)
D = 0.22235 + 0.033222 ln(AlIV)
D = -0.31053 + 1.6115 (AlIV)
a
DF cpx/L
AlIV in clinopyroxene

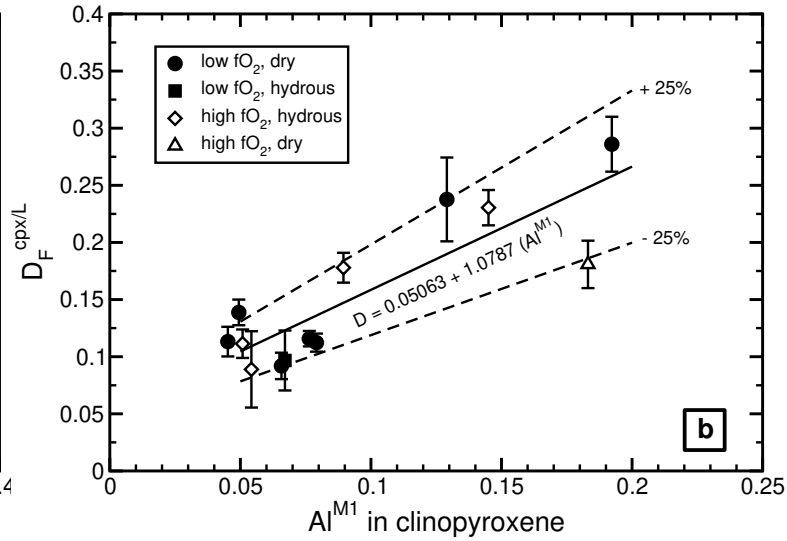
low fO2, dry
low fO2, hydrous
high fO2, hydrous
high fO2, dry
+ 25%
- 25%
D = 0.05063 + 1.0787 (AlM1)
b
DF cpx/L
AlM1 in clinopyroxene

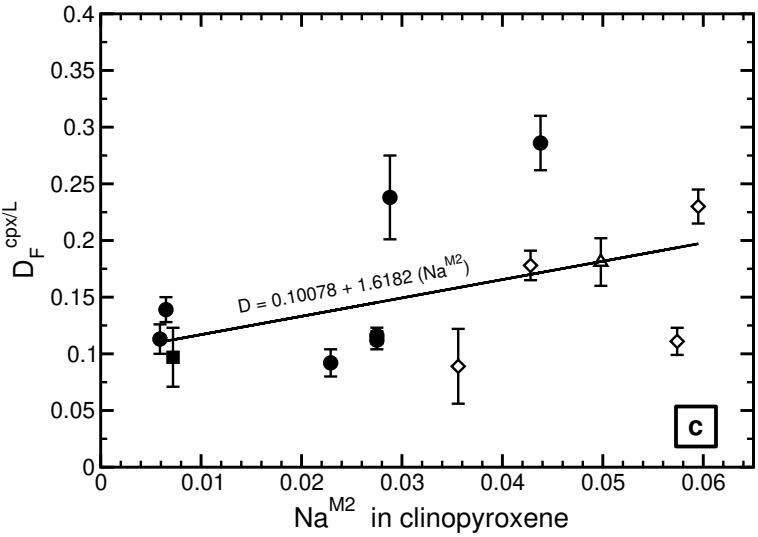
D = 0.10078 + 1.6182 (NaM2)
c
DF cpx/L
NaM2 in clinopyroxene

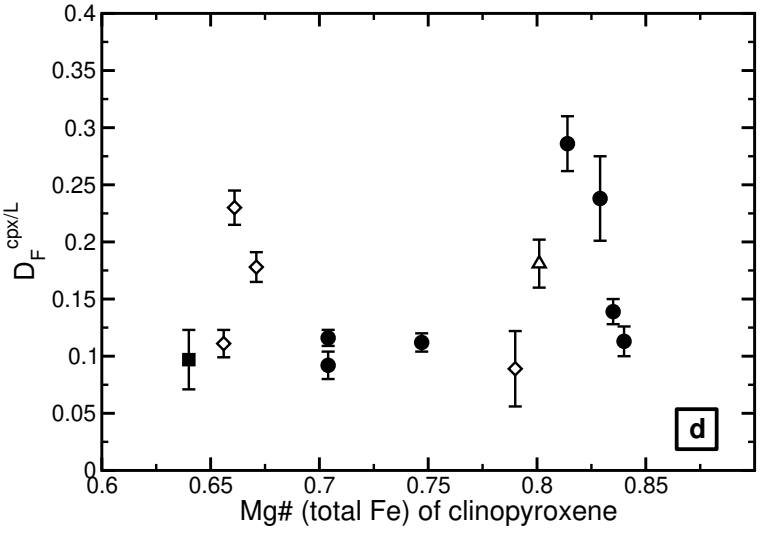
d
DF cpx/L
Mg# (total Fe) of clinopyroxene

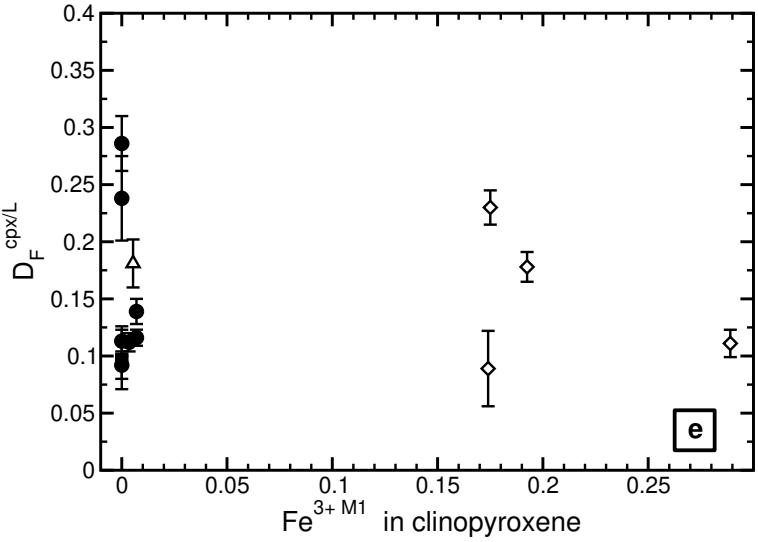
e
DF cpx/L
Fe3+ M1 in clinopyroxene

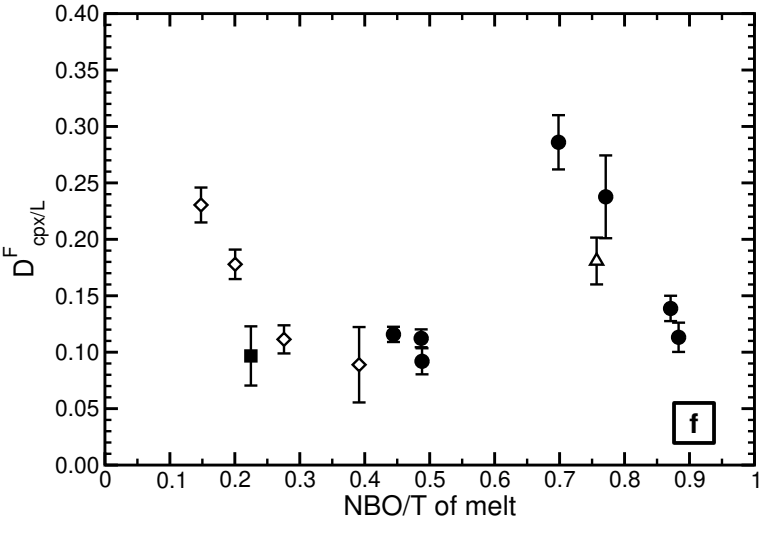
f
DF cpx/L
NBO/T of melt

Figure 2

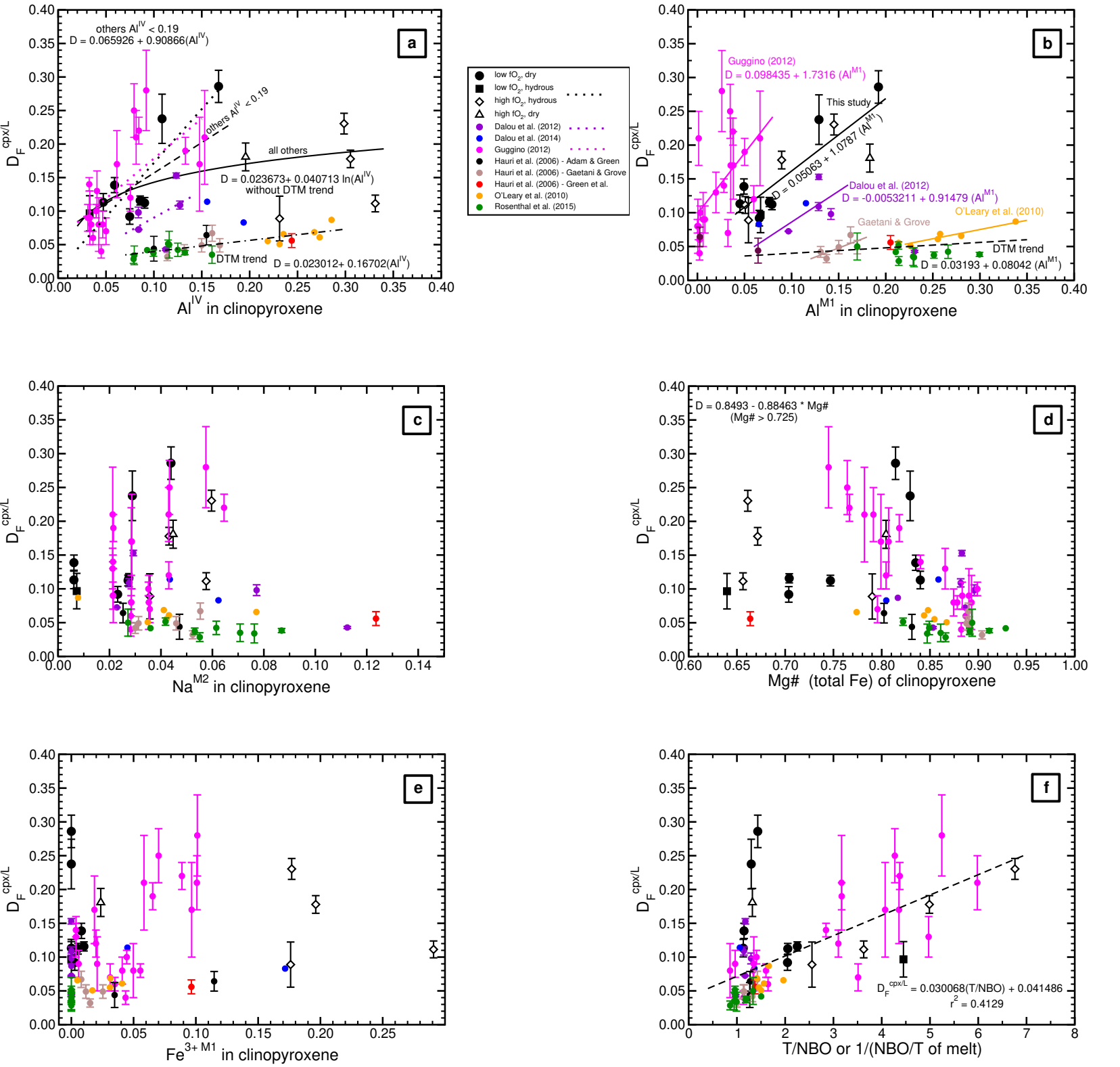
a
others Al^{IV} < 0.19
D = 0.065926 + 0.90866(Al^{IV})
others Al^{IV} < 0.19
all others
D = 0.023673+ 0.040713 ln(Al^{IV})
without DTM trend
DTM trend
D = 0.023012+ 0.16702(Al^{IV})
$D_F^{cpx/L}$
Al^{IV} in clinopyroxene
low fO_2, dry
low fO_2, hydrous
high fO_2, hydrous
high fO_2, dry
Dalou et al. (2012)
Dalou et al. (2014)
Guggino (2012)
Hauri et al. (2006) - Adam & Green
Hauri et al. (2006) - Gaetani & Grove
Hauri et al. (2006) - Green et al.
O'Leary et al. (2010)
Rosenthal et al. (2015)
b
Guggino (2012)
D = 0.098435 + 1.7316 (Al^{M1})
This study
D = 0.05063 + 1.0787 (Al^{M1})
Dalou et al. (2012)
D = -0.0053211 + 0.91479 (Al^{M1})
Gaetani & Grove
O'Leary et al. (2010)
DTM trend
D = 0.03193 + 0.08042 (Al^{M1})
Al^{M1} in clinopyroxene
c
Na^{M2} in clinopyroxene
d
D = 0.8493 - 0.88463 * Mg#
(Mg# > 0.725)
Mg# (total Fe) of clinopyroxene
e
$Fe^{3+\ M1}$ in clinopyroxene
f
$D_F^{cpx/L}$ = 0.030068(T/NBO) + 0.041486
r^2 = 0.4129
T/NBO or 1/(NBO/T of melt)

Figure 3

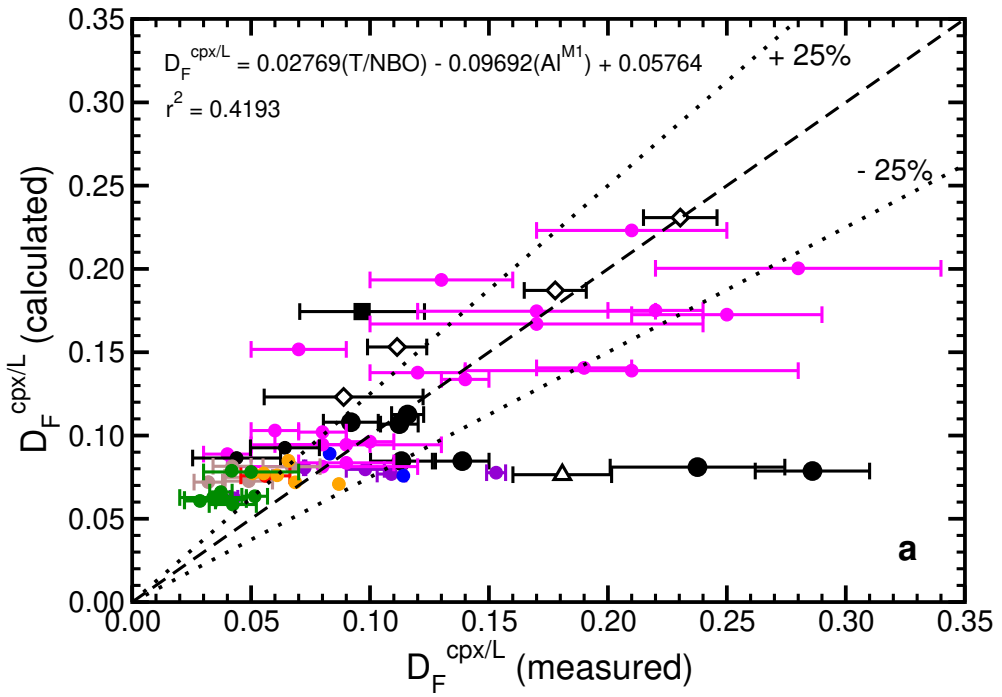
$D_F^{cpx/L}$ = 0.02769(T/NBO) - 0.09692(Al^{M1}) + 0.05764
r^2 = 0.4193
+ 25%
- 25%
a
$D_F^{cpx/L}$ (calculated)
$D_F^{cpx/L}$ (measured)

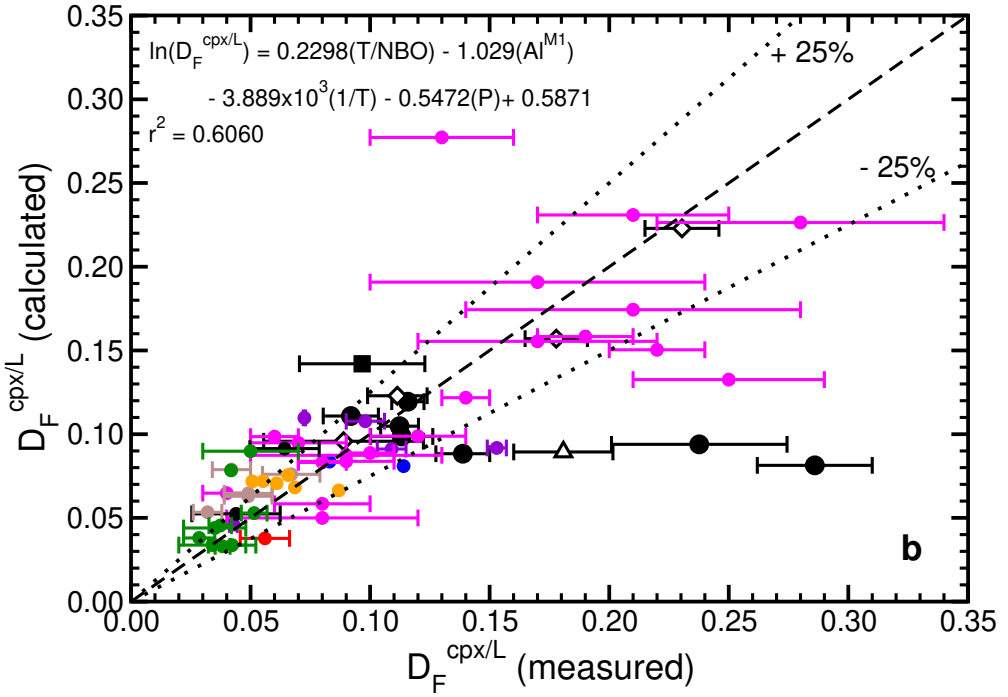
$\ln(D_F^{cpx/L})$ = 0.2298(T/NBO) - 1.029(Al^{M1})
- 3.889x10^3(1/T) - 0.5472(P)+ 0.5871
r^2 = 0.6060
+ 25%
- 25%
b
$D_F^{cpx/L}$ (calculated)
$D_F^{cpx/L}$ (measured)

Figure 4

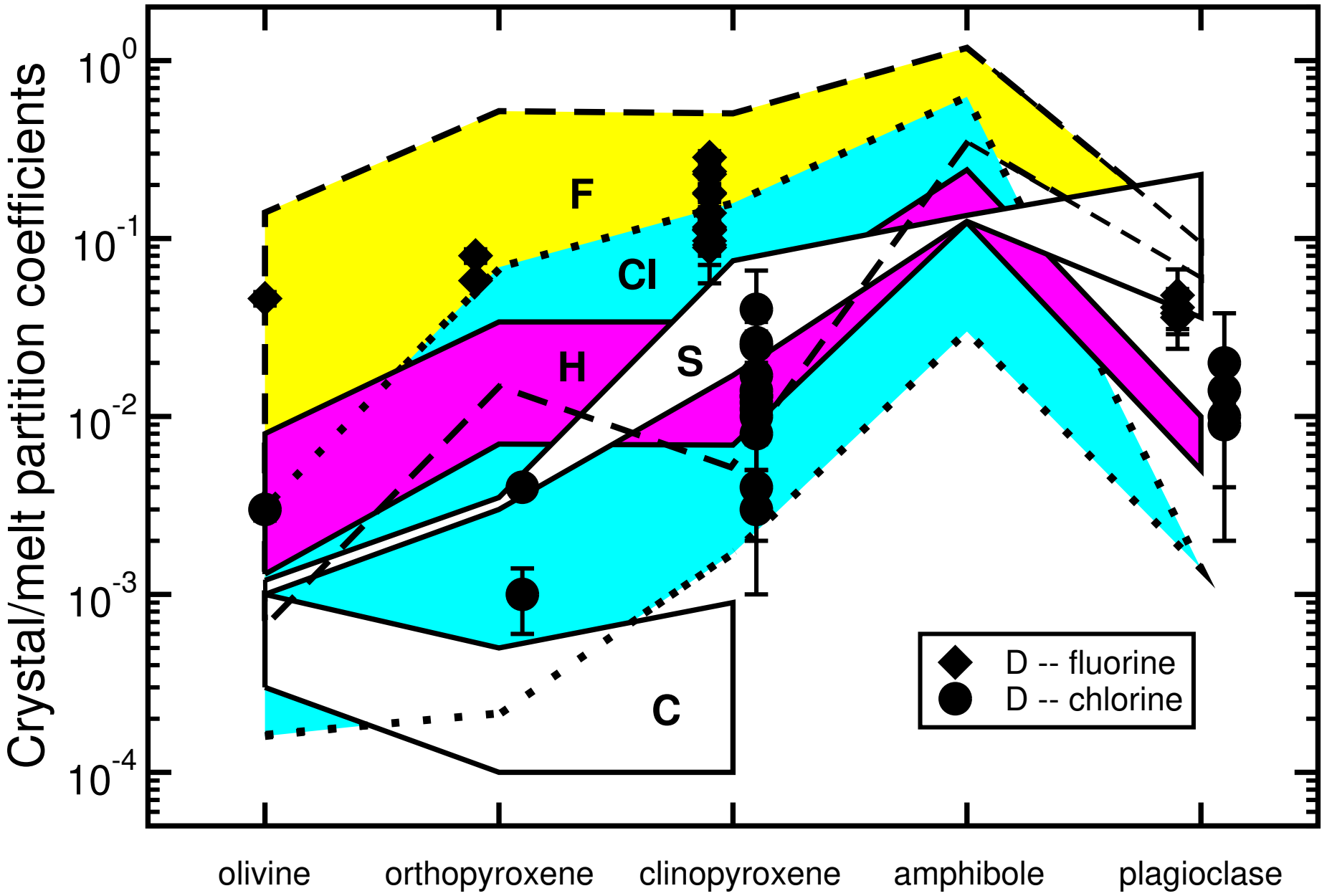
Crystal/melt partition coefficients
10^{0}
10^{-1}
10^{-2}
10^{-3}
10^{-4}
F
Cl
H
S
C
D -- fluorine
D -- chlorine
olivine
orthopyroxene
clinopyroxene
amphibole
plagioclase

Figure 5